IOVS Papers in Press. Published on November 8, 2012 as Manuscript iovs.12-11087

The Effect of Cone Opsin Mutations on Retinal Structure and the Integrity of the Photoreceptor Mosaic

Joseph Carroll[1,2,3,4,*], Alfredo Dubra[1,3,4,5,6], Jessica C. Gardner[7], Liliana Mizrahi-Meissonnier[8], Robert F. Cooper[9], Adam M. Dubis[2], Rick Nordgren[1], Mohamed Genead[10,11], Thomas B. Connor, Jr.[1], Kimberly E. Stepien[1], Dror Sharon[8], David M. Hunt[7,12], Eyal Banin[8], Alison J. Hardcastle[7], Anthony T. Moore[7,13], David R. Williams[5,6], Gerald Fishman[10,11], Jay Neitz[14], Maureen Neitz[14], Michel Michaelides[7,13,*]

[1]Department of Ophthalmology, Medical College of Wisconsin, 925 N. 87th Street, Milwaukee, WI 53226 USA
[2]Department of Cell Biology, Neurobiology, & Anatomy, 8701 Watertown Plank Road, Medical College of Wisconsin, Milwaukee, WI 53226 USA
[3]Department of Biophysics, 8701 Watertown Plank Road, Medical College of Wisconsin, Milwaukee, WI 53226 USA
[4]*These Authors Contributed Equally to This Work*
[5]Flaum Eye Institute, University of Rochester, 210 Crittenden Boulevard, Rochester, NY, 14642 USA
[6]Center for Visual Science, University of Rochester, RC Box 270270, Rochester, NY 14627 USA
[7]UCL Institute of Ophthalmology, 11-43 Bath Street, London, EC1V 9EL United Kingdom
[8]Department of Ophthalmology, Hadassah-Hebrew University Medical Center, Jerusalem, 91120 Israel
[9]Department of Biomedical Engineering, Marquette University, Milwaukee, WI 53223
[10]Chicago Lighthouse for People Who Are Blind or Visually Impaired, 1850 West Roosevelt Road, Chicago, IL 60608 USA
[11]Department of Ophthalmology and Visual Sciences, University of Illinois-Chicago, 1855 West Taylor Street, Chicago, IL 60612 USA
[12]School of Animal Biology & Lions Eye Institute, University of Western Australia, Perth, 6009 Australia
[13]Moorfields Eye Hospital, 162 City Road, London, EC1V 2PD United Kingdom
[14]Department of Ophthalmology, University of Washington, 325 Ninth Avenue, Seattle, WA 98104 USA

[*]*Corresponding Authors:*

Joseph Carroll
The Eye Institute
Medical College of Wisconsin
925 N. 87th Street
Milwaukee, WI 53226 USA
Phone: 1-414-456-2052
E-mail: jcarroll@mcw.edu

Michel Michaelides
University College London
Institute of Ophthalmology
11-43 Bath Street
London, EC1V 9EL, United Kingdom
Phone: +44 207 608 6864
E-mail: michel.michaelides@ucl.ac.uk

Number of Figures: 7, **Number of Tables**: 1, **Word Count**: 3,608

Conflict of Interest: D.R.W. holds patents on adaptive optics imaging.

Funding: Supported by NEI Grants P30 EY001931 (JC), R01 EY017607 (JC), T32 EY014537 (AMD), UL1 RR031973 (KES, JC), R01 EY014375 (DRW), P30 EY001319 (DRW), P30 EY001730 (MN, JN), R01 EY009303 (MN), & R01 EY009620 (JN). J. Carroll & A. Dubra are recipients of Career Development Awards from Research to Prevent Blindness. A. Dubra is the recipient of a Career Award at the Scientific Interface from the Burroughs Wellcome Fund. M. Michaelides is a recipient of a Career Development Award from the Foundation Fighting Blindness. Supported by grants from the Gene and Ruth Posner Foundation (JC), Foundation Fighting Blindness (JC, MM), The E. Matilda Ziegler Foundation for the Blind (JC), the RD & Linda Peters Foundation (JC), unrestricted departmental grants from Research to Prevent Blindness (Medical College of Wisconsin, University of Washington, University of Illinois-Chicago), the Juvenile Diabetes Research Foundation (8-2002-130), Fight for Sight UK (AJH, MM), Moorfields Eye Hospital Special Trustees (AJH, MM), and the National Institute for Health Research Biomedical Research Centre at Moorfields Eye Hospital NHS Foundation Trust and UCL Institute of Ophthalmology (AJH, ATM, MM). This study was supported in part by grant no. 3000003241 from the Chief Scientist Office of the Ministry of Health, Israel and the Yedidut Research Grant (DS, EB). This investigation was conducted in part in a facility constructed with support from the Research Facilities Improvement Program; grant number C06 RR016511 from the National Center for Research Resources, NIH.

ABSTRACT

Purpose: To evaluate retinal structure and photoreceptor mosaic integrity in subjects with *OPN1LW* and *OPN1MW* mutations.

Methods: Eleven subjects were recruited, eight of whom were previously described. Cone and rod density was measured using images of the photoreceptor mosaic obtained from an adaptive optics scanning laser ophthalmoscope (AOSLO). Total retinal thickness, inner retinal thickness, and outer nuclear layer thickness (ONL) were measured using cross-sectional spectral domain optical coherence tomography (SD-OCT) images. Molecular genetic analyses was performed to characterize the *OPN1LW* / *OPN1MW* gene array.

Results: While disruptions in retinal lamination and cone mosaic structure were observed in all subjects, genotype-specific differences were observed. For example, subjects with "L/M interchange" mutations resulting from intermixing of ancestral *OPN1LW* and *OPN1MW* genes had significant residual cone structure in the parafovea (~25% of normal), despite widespread retinal disruption that included a large foveal lesion and thinning of the parafoveal inner retina. These subjects also reported a later-onset, progressive loss of visual function. In contrast, subjects with the C203R missense mutation presented with congenital blue cone monochromacy, with retinal lamination defects being restricted to the ONL and the degree of residual cone structure (8% of normal) being consistent with that expected for the S cone submosaic.

Conclusions: The photoreceptor phenotype associated with *OPN1LW* and *OPN1MW* mutations is highly variable. These findings have implications for the potential restoration of visual function in subjects with opsin mutations. Our study highlights the importance of high-resolution phenotyping to characterize cellular structure in inherited retinal disease; such information will be critical for selecting patients most likely to respond to therapeutic intervention and for establishing a baseline for evaluating treatment efficacy.

Introduction

Mutations in the long-wavelength (L) and middle-wavelength (M) cone opsin genes (designated *OPN1LW* and *OPN1MW*, respectively) have been associated with a wide range of visual defects including red-green color vision deficiency, blue cone monochromacy (BCM), X-linked cone dystrophy, X-linked cone dysfunction, and high myopia with abnormal cone function.[1-16] While characterization of visual function in these individuals is relatively straightforward, less is known about how the presence of *OPN1LW* and *OPN1MW* mutations affect retinal structure. Such information will be of paramount importance for advancing efforts to restore cone function in individuals with *OPN1LW* and *OPN1MW* mutations.

Recent studies have shown that *OPN1LW* and *OPN1MW* mutations resulting in congenital red-green color vision defects are associated with a variable retinal phenotype, with some individuals showing disrupted cone structure and/or thinning of the outer nuclear layer (ONL).[8, 14, 17, 18] It is difficult to draw definite conclusions about the pathogenicity of a specific mutant from comparisons of these individuals, as there may be other factors influencing the retinal phenotype. For example, during development, there is competition between the first two genes in the X-chromosome opsin array in the nascent L/M cones that ends with only one of the two genes being expressed in each cell.[19] It has been shown that the relative proportion of cones expressing each of the two genes in the L/M array varies widely (over 40-fold).[20, 21] Thus previously observed differences in retinal phenotype may be confounded by differences in the relative expression of the mutant opsin with respect to the normal opsin. As the degree of retained cone photoreceptor structure will be related to the therapeutic potential of a given retina,[22] elucidation of genotype-specific retinal phenotypes is essential.

In one of the more serious vision disorders associated with *OPN1LW* and *OPN1MW* mutations, a single type of mutant opsin is expressed in all the cones that would have been L or M in a normal eye. In these subjects, rods and short-wavelength (S) cones are the only

photoreceptors expressing normal photopigments. These individuals offer the opportunity to directly evaluate the effect of different *OPN1LW* and *OPN1MW* mutations. These mutations can be placed into one of three categories: **1)** mutations that produced random non-homologous missense substitutions at single amino acid positions;[1, 3, 12, 16] **2)** partial or complete deletion of an exon;[15, 23] and **3)** a recently identified category involving intermixing of ancestral *OPN1LW* and *OPN1MW* genes to produce "L/M interchange" mutations with deleterious combinations of nucleotides at normal polymorphic positions.[7, 8, 10, 13] While at least one L/M interchange mutation has been shown to directly cause cone malfunction (Greenwald SH, et al. *IOVS* 2012; 53:ARVO E-Abstract 4643), it was recently shown that in addition to any functional changes in the photopigment caused by the mutations, many of the L/M interchange mutations also interfere with recognition of exon 3 by the splicing mechanism.[24] Some of the variants incompletely interfere with splicing, so both full length mRNA is produced as well as the inappropriately spliced transcript. Whether there are structural differences between the mutation categories, or for different mutations within a category, has been unknown.

Here we used adaptive optics scanning laser ophthalmoscopy (AOSLO) and spectral-domain optical coherence tomography (SD-OCT) to examine 11 subjects for whom all cones, except the S cones, express one of six mutant opsins. There were differences in the anatomy and in the course and severity of vision loss across mutation categories. The subjects with L/M interchange mutations reported a later-onset progressive loss of visual function, while those with the C203R mutation showed a typical congenital BCM phenotype. We observed significant disruption of retinal lamination and of cone mosaic topography in all subjects, though the degree of disruption was generally greater for subjects with L/M interchange mutations than those with random mutations. These differences provide insight into the underlying mechanisms responsible for loss of structure and function in these subjects. Furthermore, while the cone loss observed would preclude success of any efforts to restore

L/M cone function using gene therapy in any of these subjects, it may be possible to develop strategies to slow or halt the degenerative changes in people harboring L/M interchange mutations.

Methods

Human Subjects

Written informed consent was obtained after the nature and possible consequences of the study were explained. This study followed the tenets of the Declaration of Helsinki and was approved by all local Ethics Committees. We examined eight subjects for whom the clinical phenotype has been previously described and three new subjects (**see Table 1 and Supplementary Material**). Two male subjects (JC_0826, 22 years; JC_0847, 23 years) with normal color vision were included for comparison, and data from two previously published normative databases were used for comparison of the SD-OCT studies. The data used for comparison against the horizontal line scans consisted of 93 subjects with an average age of 25.7 ± 8.2 years[14] and the data used for comparison against the topographical thickness maps consisted of 60 subjects with an average age of 29 ± 8.42 years.[25] Axial length measurements were obtained on all subjects (Zeiss IOL Master; Carl Zeiss Meditec, Dublin CA), in order to determine the scale (in microns per pixel) of each retinal image. Prior to all retinal imaging, each eye was dilated and cycloplegia was induced through topical application of a combination of phenylephrine hydrochloride (2.5%) and tropicamide (1%).

Molecular Genetics

For the 3 newly recruited subjects, DNA was isolated from whole blood, and the opsin genes were amplified and sequenced using previously described methods.[7]

Spectral Domain Optical Coherence Tomography (SD-OCT)

Volumetric images of the macula were obtained using high-definition OCT (Cirrus HD-OCT; Carl Zeiss Meditec, Dublin, CA). Volumes were nominally 6 mm x 6 mm and consisted of 128 B-scans (512 A-scans / B-scan). Retinal thickness was calculated using the Macular Analysis software on the Cirrus (software version 5.0), which is automatically determined by measuring the difference between the inner limiting membrane (ILM) and RPE boundaries. High-resolution SD-OCT images of the macula were acquired (Bioptigen; Research Triangle Park, NC). High-density line scans (1000 A-scans / B-scan, 100 repeated B scans) were acquired through the foveal center, then registered and averaged as previously described.[26] No transformation (*i.e*., flattening), filtering, or other post-processing was applied to these images.

For retinal sub-layer analysis, we manually segmented the ILM, the outer plexiform layer (OPL), the external limiting membrane (ELM), and the RPE on the high-resolution line scans as previously described using ImageJ.[14] The ILM-RPE distance provides total retinal thickness, the ILM-OPL distance provides the inner retinal thickness, and the OPL-ELM distance provides the ONL plus Henle Fiber layer thickness (ONL+HFL).

Adaptive Optics Retinal Imaging

An adaptive optics scanning light ophthalmoscope (AOSLO) was used to obtain images of the photoreceptor mosaic at various retinal locations. JC_0183, JC_0184, JC_0440, JC_0441, JC_0355, JC_0356, JC_0118, and JC_0430 were imaged at the University of Rochester, details of this imaging system have been previously published.[27] The remaining 3 subjects and the normal controls were imaged at the Medical College of Wisconsin, and details of this system have also been published.[28] The systems derive from the basic design described by Gray *et al*.,[29] with the afocal telescopes folded to varying degrees.[27] Both systems utilized a 97-channel deformable mirror (ALPAO, Biviers, France) was used as the wavefront corrector,

with a Shack-Hartman wavefront sensor used to measure the wavefront. The imaging source was either a 775nm or 796nm super luminescent diode (Inphenix Inc., Livermore, CA), and the light exposure was kept below the safe maximum permissible exposure set forth by ANSI.[30, 31] Images were processed to remove distortions induced by the sinusoidal motion of the resonant scanner by estimating the distortion from images of a calibrated Ronchi ruling and then re-sampling the images over a grid of equally spaced pixels. A separate calibration was done for each subject. Images were registered to improve signal-to-noise as previously described.[32]

The registered images from each subject were combined into a single montage (Adobe Photoshop; Adobe Systems, Inc., San Jose, CA). This montage was scaled and aligned to the LSO image from the HD-OCT, in which a crosshair was placed at the center of the foveal pit. The scaling was based on theoretical magnification of each system and the alignment performed using blood vessel patterns. The locations to be analyzed were determined based on the distance from the center of the foveal pit, and the original image comprising that portion of the montage was set aside for subsequent density analyses. Cone density was measured at selected retinal locations (0.4, 0.8, 1.2, 1.6, 2.0 mm) using manual identification of cone structures (80 μm x 80 μm sampling window). For rod analysis, we utilized a smaller sampling window (55 μm x 55 μm) than we did for the cone density analysis, as the cones in these subjects were more sparse and irregularly spaced. Rod density was calculated at various locations between 0.5 and 3mm using a previously described semi-automated algorithm in which the user could add/subtract missed or erroneous cell identifications.[33]

Results

Different Genotype Classes Associated with Distinct Clinical Phenotypes **Table 1** provides a summary of subject demographics, with the clinical phenotype on 8/11 having been reported previously. All four subjects with C203R mutations and the subject with the exon 2

deletion presented a classical BCM phenotype, with vision based solely on S cones and rods.[12, 15] The two brothers with W177R mutations (JC_0355 & JC_0356) had an onset in the first decade, with subsequent deterioration of visual acuity and color vision, had no history of nystagmus, macular retinal pigment epithelial disturbance, and severe generalized cone dysfunction on ERG.[16] Both had good S-cone function with absent L/M cone function on psychophysical testing, though the data could not entirely exclude some residual L/M cone function in JC_0355.[16]

The remaining four subjects (JC_0347, JC_0564, JC_0118, KS_0577) had *OPN1LW* and *OPN1MW* mutations that fell into the newly discovered category involving intermixing of ancestral genes to produce "L/M interchange" mutations with deleterious combinations of nucleotides at normal polymorphic positions in exon 3.[7, 8, 10, 13, 19, 24] All 4 of these subjects had a late-onset, progressive phenotype that was in stark contrast to that of the subjects with a C203R mutation or the exon 2 deletion (see **Supplementary Material**). While the subjects with W177R mutations also had a progressive phenotype, it was earlier onset than that observed for the L/M interchange mutations and resulted in more complete loss of L/M cone function.

Reduced Retinal Thickness in Subjects with OPN1LW and OPN1MW Mutations

Topographical maps of retinal thickness show variable but significant macular thinning in individuals with all three classes of mutation (**Fig. S1**). The average (± SD) central subfield (CSF) thickness (central 1mm) for the 11 subjects examined here was 194 ± 34 μm, compared to an average (± SD) value for 60 normal subjects from our lab of 266 ± 19 μm;[25] $p<0.0001$, Mann-Whitney Test. The subjects with random point mutations had more normal CSF thickness (216 ± 20 μm) than the individuals with L/M interchange mutations (174 ± 28 μm);

p=0.0381, Mann-Whitney Test. In addition, the retinal thinning in the subjects with L/M interchange mutations was more widespread (**Fig. S1**).

To investigate the reduction in retinal thickness in more detail, we examined the thickness of the inner retina and the ONL+HFL from high-resolution horizontal cross-sections (**Fig. 1**), and compared it to previously reported normative data.[14] Consistent with the topographical thickness analysis, we observed that subjects with random point mutations had more normal total retinal thickness than subjects in the other two genetic categories (**Fig. 2A**). However, subjects with random point mutations had thinning restricted to the ONL+HFL, while subjects with L/M interchange mutations (LVAVA, LIAVS and LVVVA) or the exon 2 deletion showed parafoveal thinning of the inner retina in addition to reduced ONL+HFL thickness (**Fig. 2B, C**).

Variable Appearance of Outer Photoreceptor Complex on SD-OCT in Subjects with OPN1LW and OPN1MW Mutations In the normal retina, four hyper-reflective bands comprise the outer photoreceptor complex (see JC_0847 in **Fig. 1**). The innermost peak of the outer photoreceptor complex is attributed to the external limiting membrane (ELM), while the 2nd layer is now thought to derive from the ellipsoid portion of the inner segment (ISe).[34] The 3rd layer is attributed to the RPE contact cylinder and the 4th band is attributed to the RPE. As shown in **Figure 2**, we observed disruption of the ISe in all subjects; however, there were differences between the mutation classes that paralleled the differences in retinal thinning. Five of the six individuals with random point mutations (JC_0183, JC_0184, JC_0440, JC_0441, and JC_0355) had a focal disruption of the ISe near the foveal center. In contrast, subjects with L/M interchange mutations had generally greater disruption of the ISe – JC_0118 (LIAVS) and KS_0577 (LVVVA) had a large area of ISe loss (as did the subject with the Exon 2 deletion, JC_0430), and JC_0564 (LVAVA) showed diffuse mottling of the ISe. However,

these differences did not segregate perfectly with genotype category, as JC_0347 (LVAVA) had a well-defined focal lesion and JC_0356 (W177R) had diffuse mottling of the ISe.

In the six individuals with the focal ISe disruption, the boundaries of the disruption were marked using Image J,[35] with the average (± SD) width being 99.2 ± 43.5 μm; consistent with previous estimates of the size of the S-cone free zone in humans.[36-38]

Disrupted Foveal Cone Mosaic in Subjects with OPN1LW and OPN1MW Mutations

Foveal montages created by stitching together multiple overlapping images are shown in **Fig. 3**. Differences between the genotypic categories parallel those observed in the SD-OCT images. We observed a hyporeflective area at or near the foveal center in the six aforementioned subjects with a focal ISe disruption on SD-OCT, consistent with this small area lacking healthy, waveguiding cones. A sparse population of hyperreflective cones, presumably S-cones, surrounded this hyporeflective area. The three subjects with a larger area of ISe loss on SD-OCT had irregular areas of hyperreflectivity in the foveal montages with minimal cone structure present consistent with disruption of L, M and S foveal cones in their macula. The remaining two subjects had more diffuse photoreceptor mosaic disruption across the foveal montage with only sporadic hyperreflective cones, in keeping with the irregularly disrupted ISe.

Shown in **Figure 4** are plots of the putative S-cones observed in the foveal montages for the 6 subjects with a discrete disruption of the ISe, compared to a plot of similar data from Curcio *et al.*[38] While the analysis may not capture every S cone, it does provide a robust way to visualize the relative absence of reflective cones in a particular region. The size of the presumed S-cone free zone was determined by finding the largest circle that could be placed within the cone mosaic without encroaching on any cones, and ranged from 50-120 μm, with an average of 72 μm for the 6 subjects. This is consistent with previous estimates of the size of the S-cone free zone, [36-38] providing further support that the focal ISe represents complete

loss of L/M cone structure in the foveola. Interestingly, the center of the presumed S-cone free zone did not always align to the center of the foveal pit.

Residual Parafoveal L/M Cone Structure in Subjects with OPN1LW and OPN1MW Mutations The parafoveal cone mosaic in subjects with *OPN1LW* and *OPN1MW* mutations is severely disrupted compared to normal (**Fig. 5**). However, there are important differences between the genetic categories. Between L/M interchange mutations and those with C203R mutations and W177R mutations, the severity of the losses are reversed compared to the foveal region. While the macula was generally thinner and the foveal region more disrupted for the interchange mutations as a group, their parafoveal cone numbers are better preserved in the parafovea (**Fig. 6**). The difference is largest at 2 millimeters from the fovea, the most eccentric location measured. We were not able to resolve the rod mosaic in all subjects, but measurements made outside the central area of ISe disruption (visible on OCT) showed rod density consistent with that measured previously in normals with the same technique (**Fig. 7**).[39]

Assuming a starting cone density equal to that of an average normal,[40] the residual density for the subjects with the random point mutations is 8.5% of normal (SD=3.0%), consistent with that expected if they had only S cones remaining.[37, 38] In contrast, the subjects with L/M interchange mutations had residual densities that were on average 23% of normal (SD=10.7%). Factoring in the expected population of S cones, we estimate that this corresponds to a loss of 86% of the L/M cones (SD=9%). As normal cone density is highly variable, it is impossible to determine the exact degree of cone loss (or the degree of cone retention); however, it is clear that the retinas harboring C203R or W177R have very few, if any, residual L/M cones. Likewise, there is certainly residual L/M cone structure in subjects with L/M interchange mutations, consistent with the residual L/M cone function measured with the ERG in KS_0577, JC_0347, & JC_0564 (Kuchenbecker J, et al. *IOVS* 2012; 53:ARVO E-

Abstract 6400). Structure/function agreement was also seen between the two subjects with the W77R mutation, where JC_0355 had higher cone density and less retinal thinning than his brother (JC_0356), consistent with him having slightly better vision in one eye and better L/M cone function on psychophysical testing.[16]

Discussion

Different Retinal Phenotypes in Subjects with OPN1LW and OPN1MW Mutations While all subjects had disrupted photoreceptor mosaics and reduced retinal thickness, there were significant differences between the mutation classes. The imaging results provide a number of insights into the basis for the observed phenotypic differences between the mutation categories. In general, the six subjects with random missense mutations (C203R and W177R) had the healthiest appearing retinas on SD-OCT. The small disruption of the ISe that was present was shown to correspond to the S-cone free zone,[36-38] with the focal loss of the ISe being the result of the absence of healthy L or M cones, S-cones, or rods to provide structure at the foveal center.

In contrast to the C203R and W177R mutations, the L/M interchange mutations (4 subjects) and exon 2 deletion (1 subject) appear to be more disruptive to the overall foveal architecture. Only 1/5 of these subjects (JC_0347, LVAVA) had a small focal disruption of the ISe, with the others having diffuse mottling of the ISe or a much larger absence of the ISe (extending into the parafovea). Compared to the subjects with the random point mutations, these subjects had greater retinal thinning that involved the inner retina as well as the ONL. This suggests that these L/M interchange mutations cause, or are associated with, degenerative changes that result in damage to neighboring cells (S cones and rods) in addition to those expressing mutant L/M opsin.

The specificity of the photoreceptor damage to the macular region in the subjects with L/M interchange mutations is striking when comparing images of the fovea to more peripheral ones. Retinoid bi-products of the visual cycle and all-trans-retinal (atRAL) are particularly toxic.[41] It is possible that the cones expressing the L/M interchange mutants remain viable through young adulthood but are defective in their ability to participate normally in the visual cycle. This could lead to a buildup of atRAL or other toxic retinoids, affecting not only the cones expressing the mutant opsin, but also parafoveal S-cones and rods. If these toxic by-products are concentrated in the fovea where the cone density is 20 times higher than in the peripheral retina,[40] it could explain why the collateral damage is higher at the central retina compared to more eccentric locations (**Fig. 1**).

Implications for Restoration of Visual Function in Subjects with OPN1LW and OPN1MW Mutations Advances in gene therapy have generated a great deal of excitement regarding the restoration of cone function in a variety of retinal diseases.[42-48] While subjects with L/M interchange mutations had the greatest degree of residual parafoveal L/M cone structure, the presence of macular atrophy and inner retinal thinning in most of these subjects would limit the therapeutic opportunity in these individuals at later stages of the disease. However, strategies may be developed to slow the degenerative effects of these mutations. In contrast, the subjects with C203R or W177R mutations generally had more preserved retinal lamination, but AO imaging revealed no evidence for retained L/M cone structure. It is unclear whether any cone cell bodies remain, though given that rods appear to have expanded to fill in the space occupied by the cones, this would imply degeneration of at least the inner and outer segments.

We did not examine subjects with LCR deletions, so it remains to be seen how complete absence of L/M opsin affects cone photoreceptor integrity compared to the expression of mutant opsin. Furthermore, we are unable to say if there are structural

differences between individuals harboring different L/M interchange mutations. Previous evidence showed that an individual with the LIAVA mutant expressed by one of the 2 genes in the L/M array had random, non-waveguiding cells throughout the cone mosaic, normal ISe integrity, normal inner retinal thickness, and no change in cone structure measured over a span of 8 years.[8, 18] This suggests the LIAVA mutant may not result in the progressive loss of L/M cones (or does so on a much slower time scale), and it will be important to longitudinally assess the progressive nature of the various L/M interchange mutations to better determine the therapeutic potential in these individuals.

In addition to using the imaging tools described here to prioritize potential subjects most suitable for intervention by characterizing the degree of residual cone structure in subjects with *OPN1LW* and *OPN1MW* mutations, it will be valuable to employ the same techniques when evaluating the safety and efficacy of any future therapeutic intervention. Such an approach has already been demonstrated in patients with retinitis pigmentosa receiving ciliary neurotrophic factor,[49] where preservation of cone structure was observed in the absence of a significant functional improvement in vision. It is entirely plausible that structural recovery or preservation precedes functional changes, however this will remain unclear until high-resolution imaging metrics become a routine part of the outcome measures used in clinical trials.

Acknowledgments

The authors thank P. Godara, Z. Harvey, J. Norris, J. Rha, N. Smith, & P. Summerfelt, for assistance with the study.

Author contributions: J.C., A.D., A.J.H., D.R.W., M.N., M.M. designed research; J.C., A.D., J.C.G, L.M., R.F.C., A.M.D., R.N., M.G., T.B.C., K.E.S., D.S., D.M.H., E.B., A.J.H., A.T.M., D.R.W., G.F., J.N., M.N., M.M. performed research; J.C., A.D., J.C.G., A.M.D., R.N., M.G., M.N., M.M. analyzed data; & J.C., M.G., T.B.C., K.E.S., D.S., E.B., A.J.H., D.R.W., G.F., J.N., M.N., M.M. wrote the paper.

References

1. Nathans J, Davenport CM, Maumenee IH, et al. Molecular genetics of human blue cone monochromacy. *Science.* 1989;**245**:831-838.
2. Winderickx J, Sanocki E, Lindsey DT, et al. Defective colour vision associated with a missense mutation in the human green visual pigment gene. *Nat Genet.* 1992;**1**:251-256.
3. Nathans J, Maumenee IA, Zrenner E, et al. Genetic heterogeneity among blue-cone monochromats. *Am J Hum Genet.* 1993;**53**:987-1000.
4. Ayyagari R, Kakuk LE, Toda Y, et al. Blue cone monochromacy: Macular degeneration in individuals with cone specific gene loss. In: Hollyfield JG, Anderson RE, LaVail MM (eds), *Retinal Degenerative Diseases and Experimental Therapy.* New York: Kluwer Academic / Plenum Publishers; 1999.
5. Jagla WM, Jägle H, Hayashi T, et al. The molecular basis of dichromatic color vision in males with multiple red and green visual pigment genes. *Hum Mol Genet.* 2002;**11**:23-32.
6. Kellner U, Wissinger B, Tippmann S, et al. Blue cone monochromatism: clinical findings in patients with mutations in the red/green opsin gene cluster. *Graefes Arch Clin Exp Ophthalmol.* 2004;**242**:729-735.
7. Neitz M, Carroll J, Renner A, et al. Variety of genotypes in males diagnosed as dichromatic on a conventional clinical anomaloscope. *Vis Neurosci.* 2004;**21**:205-216.
8. Carroll J, Neitz M, Hofer H, et al. Functional photoreceptor loss revealed with adaptive optics: An alternate cause for color blindness. *Proc Natl Acad Sci USA.* 2004;**101**:8461-8466.
9. Young TL, Deeb SS, Ronan SM, et al. X-linked high myopia associated with cone dysfunction. *Arch Ophthalmol.* 2004;**122**:897-908.
10. Crognale MA, Fry M, Highsmith J, et al. Characterization of a novel form of X-linked incomplete achromatopsia. *Vis Neurosci.* 2004;**21**:197-203.
11. Michaelides M, Johnson S, Bradshaw K, et al. X-linked cone dysfunction syndrome with myopia and protanopia. *Ophthalmology.* 2005;**112**:1448-1454.
12. Michaelides M, Johnson S, Simunovic MP, et al. Blue cone monochromatism: a phenotype and genotype assessment with evidence of progressive loss of cone function in older individuals. *Eye.* 2005;**19**:2-10.
13. Mizrahi-Meissonnier L, Merin S, Banin E, Sharon D. Variable retinal phenotypes caused by mutations in the X-linked photopigment gene array. *Invest Ophthalmol Vis Sci.* 2010;**51**:3884-3892.
14. Carroll J, Baraas RC, Wagner-Schuman M, et al. Cone photoreceptor mosaic disruption associated with Cys203Arg mutation in the M-cone opsin. *Proc Natl Acad Sci USA.* 2009;**106**:20948-20953.
15. Gardner JC, Michaelides M, Holder GE, et al. Blue cone monochromacy: Causative mutations and associated phenotypes. *Mol Vis.* 2009;**15**:876-884.
16. Gardner JC, Webb TR, Kanuga N, et al. X-linked cone dystrophy caused by mutation of the red and green cone opsins. *Am J Hum Genet.* 2010;**87**:26-39.
17. Wagner-Schuman M, Neitz J, Rha J, et al. Color-deficient cone mosaics associated with Xq28 opsin mutations: a stop codon versus gene deletions. *Vision Res.* 2010;**50**:2396-2402.
18. Rha J, Dubis AM, Wagner-Schuman M, et al. Spectral domain optical coherence tomography and adaptive optics: Imaging photoreceptor layer morphology to interpret preclinical phenotypes. *Adv Exp Med Biol.* 2010;**664**:309-316.
19. Neitz J, Neitz M. The genetics of normal and defective color vision. *Vision Res.* 2011;**51**:633-651.
20. Carroll J, Neitz M, Neitz J. Estimates of L:M cone ratio from ERG flicker photometry and genetics. *J Vision.* 2002;**2**:531-542.

21. Hofer H, Carroll J, Neitz J, et al. Organization of the human trichromatic cone mosaic. *J Neurosci.* 2005;**25**:9669-9679.
22. Jacobson SG, Aleman TS, Cideciyan AV, et al. Identifying photoreceptors in blind eyes caused by RPE65 mutations: Prerequisite for human gene therapy success. *Proc Natl Acad Sci USA.* 2005;**102**:6177-6182.
23. Ladekjaer-Mikkelsen A-S, Rosenberg T, Jørgensen AL. A new mechanism in blue cone monochromatism. *Hum Genet.* 1996;**98**:403-408.
24. Ueyama H, Muraki-Oda S, TYamade S, et al. Unique haplotype in exon 3 of cone opsin mRNA affects splicing of its precursor, leading to congenital color vision defect. *Biochem Biophys Res Commun.* 2012;**424**:152-157.
25. Wagner-Schuman M, Dubis AM, Nordgren RN, et al. Race- and sex-related differences in retinal thickness and foveal pit morphology. *Invest Ophthalmol Vis Sci.* 2010;**52**:625-634.
26. Tanna H, Dubis AM, Ayub N, et al. Retinal imaging using commercial broadband optical coherence tomography. *Br J Ophthalmol.* 2010;**94**:372-376.
27. Dubra A, Sulai Y. Reflective afocal broadband adaptive optics scanning ophthalmoscope. *Biomed Opt Express.* 2011;**2**:1757-1768.
28. Cooper RF, Dubis AM, Pavaskar A, et al. Spatial and temporal variation of rod photoreceptor reflectance in the human retina. *Biomed Opt Express.* 2011;**2**:2577-2589.
29. Gray DC, Merigan W, Wolfing JI, et al. In vivo fluorescence imaging of primate retinal ganglion cells and retinal pigment epithelial cells. *Opt Express.* 2006;**14**:7144-7158.
30. ANSI. American National Standard for Safe Use of Lasers (ANSI Z136.1). *ANSI Z1361-2007*: The Laser Institute of America; 2007.
31. Delori FC, Webb RH, Sliney DH, Institute ANS. Maximum permissible exposures for ocular safety (ANSI 2000), with emphasis on ophthalmic devices. *J Opt Soc Am A.* 2007;**24**:1250-1265.
32. Dubra A, Harvey Z. Registration of 2D Images from Fast Scanning Ophthalmic Instruments *The 4th International Workshop on Biomedical Image Registration.* Lübeck, Germany; 2010.
33. Garrioch R, Langlo C, Dubis AM, et al. Repeatability of in vivo parafoveal cone density and spacing measurements. *Optom Vis Sci.* 2012;**89**:632-643.
34. Spaide RF, Curcio CA. Anatomical correlates to the bands seen in the outer retina by optical coherence tomography: literature review and model. *Retina.* 2011;**31**:1609-1619.
35. Abramoff MD, Magelhaes PJ, Ram SJ. Image processing with ImageJ. *Biophotonics International.* 2004;**11**:36-42.
36. Williams DR, MacLeod DIA, Hayhoe MM. Punctate sensitivity of the blue-sensitive mechanism. *Vision Res.* 1981;**21**:1357-1375.
37. Ahnelt PK, Kolb H, Pflug R. Identification of a subtype of cone photoreceptor, likely to be blue sensitive, in the human retina. *J Comp Neurol.* 1987;**255**:18-34.
38. Curcio CA, Allen KA, Sloan KR, et al. Distribution and morphology of human cone photoreceptors stained with anti-blue opsin. *J Comp Neurol.* 1991;**312**:610-624.
39. Dubra A, Sulai Y, Norris JL, et al. Non-invasive imaging of the human rod photoreceptor mosaic using a confocal adaptive optics scanning ophthalmoscope. *Biomed Opt Express.* 2011;**2**:1864-1876.
40. Curcio CA, Sloan KR, Kalina RE, Hendrickson AE. Human photoreceptor topography. *J Comp Neurol.* 1990;**292**:497-523.
41. Chen Y, Okano K, Maeda T, et al. Mechanism of all-trans-retinal toxicity with implications for stargardt disease and age-related macular degeneration. *J Biol Chem.* 2012;**287**:5059-5069.
42. Alexander JJ, Umino Y, Everhart D, et al. Restoration of cone vision in a mouse model of achromatopsia. *Nat Med.* 2007;**13**:685-687.
43. Maguire AM, Simonelli F, Pierce EA, et al. Safety and efficacy of gene transfer for Leber's congenital amaurosis. *N Engl J Med.* 2008;**358**:2240-2248.

44. Bainbridge JW, Smith AJ, Barker SS, et al. Effect of gene therapy on visual function in Leber's congenital amaurosis. *N Engl J Med.* 2008;**358**:2231-2239.
45. Cideciyan AV, Aleman TS, Boye SL, et al. Human gene therapy for RPE65 isomerase deficiency activates the retinoid cycle of vision but with slow rod kinetics. *Proc Nat Acad Sci USA.* 2008;**105**:15112-15117.
46. Mancuso K, Hauswirth WW, Li Q, et al. Gene therapy for red-green colour blindness in adult primates. *Nature.* 2009;**461**:784-787.
47. Komáromy A, Alexander JJ, Rowlan JS, et al. Gene therapy rescues cone function in congenital achromatopsia. *Hum Mol Genet.* 2010;**19**:2581-2593.
48. Carvalho LS, Xu J, Pearson R, et al. Long-term and age-dependent restoration of visual function in a mouse model of CNGB3-associated achromatopsia following gene therapy. *Hum Mol Genet.* 2011;**20**:3161-3175.
49. Talcott KE, Ratnam K, Sundquist S, et al. Longitudinal study of cone photoreceptors during retinal degeneration and in response to ciliary neurotrophic factor treatment. *Invest Ophthalmol Vis Sci.* 2011;**52**:2219-2226.

Figure Legends

Figure 1. SD-OCT images (horizontal line scans) through the fovea. Images are labeled with the subject ID and corresponding genotype. An image from a normal control (JC_0847) is shown for comparison (*lower right*). Four layers (labeled on the normal control scan) are associated with the hyperreflective photoreceptor complex, with layer 1 being attributed to the ELM and layer 2 to the ellipsoid portion of the inner segment (ISe). Layers 3 and 4 are thought to originate from different aspects of the RPE/photoreceptor interface and RPE, respectively.[34] Variable disruption of the ISe was observed across the 11 subjects. Scale bar is 200 μm.

Figure 2. Retinal thickness analysis along the horizontal meridian. (A) Total retinal thickness, (B) ONL+HFL thickness, (C) inner retinal thickness. Solid black line represents mean values for 93 normal controls, with shaded region representing ±2 standard deviations from the mean. Filled circles represent averaged data for the C203R subjects (JC_0183, JC_0184, JC_0440, JC_0441), filled triangles represent averaged data for the W177R subjects (JC_0355, JC_0356), filled squares represent averaged data for the LVAVA subjects (JC_0347, JC_0564), open circles represent data for the LIAVS subject (JC_0118), open triangles

represent data for the LVVVA subject (KS_0577), and open squares represent data for the subject with the exon 2 deletion (JC_0430). All subjects showed significant retinal thinning (total and ONL+HFL) with only the C203R and W177R subjects having normal inner-retinal thickness.

Figure 3. Variable disruption of the central photoreceptor mosaic. AOSLO montages of the photoreceptor mosaic are shown, created by stitching together multiple overlapping images. The location of the foveal pit is marked with an asterisk, and the orientation of the montages is provided at the lower right (S=superior, I=inferior, N=nasal, T=temporal). The location and extent of disruption visualized in the AOSLO montages was consistent with that seen on the SD-OCT images. Scale bar is 100 μm.

Figure 4. Visualizing the S-cone free zone. Shown are plots of putative S-cones observed in the foveal montages for the 6 subjects with a discrete disruption of the ISe, compared to a plot of similar data from Curcio *et al.*[38] Filled circles are manually identified cones near the foveal center, identified by their bright, Gaussian reflective profile. Open squares represent the center of the foveal pit, and it is worth noting that the center of the presumed S-cone free zone does not always align to the center of the foveal pit. The analysis may not capture every S cone, and thus may not provide accurate estimates of S-cone density, however it does provide a robust way to map the relative absence of reflective cones in a particular region. The size of the presumed S-cone free zone was determined by finding the largest circle that could be placed within the cone mosaic without encroaching on any cones, and ranged from 50-120 μm, with an average of 72 μm for the 6 subjects. Scale bar is 100 μm.

Figure 5. Disruption of the parafoveal photoreceptor mosaic. Eccentricity-matched images from a normal (*left*) compared to those from four of the mutations studied here (*middle* and *right*) are shown. The eccentricity of each image is given as the distance from the foveal center. In the normal images, cones are the larger structures and rods the smaller ones. In the subjects with *OPN1LW* and *OPN1MW* mutations, there are fewer cones compared to normal and the rods appear larger, but still comprise a contiguous mosaic. Scale bar is 50 μm.

Figure 6. Genotype-dependent differences in retained cone structure. Solid gray bars represent the minimum and maximum S-cone density values reported in a previous histology study.[38] Solid black bars represent averaged data for the C203R subjects (JC_0183, JC_0184, JC_0440, JC_0441), while the open bars represent averaged data for the W177R subjects (JC_0355, JC_0356). Filled squares represent averaged data for the LVAVA subjects (JC_0347, JC_0564), open circles represent data for the LIAVS subject (JC_0118), open triangles represent data for the LVVVA subject (KS_0577), and the open square represents data for the subject with the exon 2 deletion (JC_0430).

Figure 7. Parafoveal rod density in subjects with *OPN1LW* and *OPN1MW* mutations. It was not possible to visualize rods in all subjects or at systematic retinal locations, but in all areas assessed (eccentric to the central ISe disruption), we observed a contiguous rod mosaic of expected density. Subjects with C203R or W177R are plotted as open squares, subjects with L/M interchange mutations are plotted as filled circles, and the crosses represent normals measured using AOSLO from a previous study.[39] The solid line is the average rod density from a previous histology report.[40]

Table 1. Clinical and genetic summary

Subject	Age, yrs	Axial Length, mm (OD, OS)	BCVA (OD, OS)	L/M Array Structure	L/M Mutation	Source*
JC_0183	16	25.65, 25.92	20/80, 20/80	0L, 1M	C203R[†]	Fam. C, V:4 (Ref. 12)
JC_0184	13	24.85, 24.76	20/120, 20/120	0L, 1M	C203R[†]	Fam. C, V:5 (Ref. 12)
JC_0440	18	25.49, 25.75	20/80, 20/80	0L, 2M	C203R[†,‡]	Fam.1, 2.1 (Ref. 15)
JC_0441	18	25.21, 25.12	20/80, 20/80	0L, 2M	C203R[†,‡]	Fam.1, 2.2 (Ref. 15)
JC_0355	31	24.54, 24.59	20/80, 20/125	1L, 1M	W177R[§,‡]	IV:1 (Ref. 16)
JC_0356	30	25.90, 25.88	20/125, 20/125	1L, 1M	W177R[§,‡]	IV:2 (Ref. 16)
JC_0347	32	24.77, 24.25	20/125, 20/125	1L, 0M	LVAVA[¶]	This Study
JC_0564	45	27.08, 26.58	20/100, 20/100	0L, 1M	LVAVA[¶]	This Study
JC_0118	32	25.83, 26.43	20/40, 20/40	1L, 0M	LIAVS[¶]	MOL0250 III:2 (Ref. 13)
KS_0577	38	23.71, 23.93	20/70, 20/100	0L, 1M	LVVVA[¶]	This Study
JC_0430	26	25.40, 25.31	20/120, 20/120	0L, 1M	Exon 2 del.	Fam. A, III:3 (Ref. 12)

*Previous report of genotype and/or phenotype.
[†]Substitution of Cysteine (C) for Arginine (R) at position 203.
[‡]Both genes in the array encode mutation.
[§]Substitution of Tryptophan (W) for Arginine at position 177.
[¶]Sequence of polymorphic amino acids encoded by exon 3 of the L/M gene present in the subjects' L/M gene array (153, 171, 174, 178,180). L=leucine, I=isoleucine, A=alanine, V=valine, S=serine.

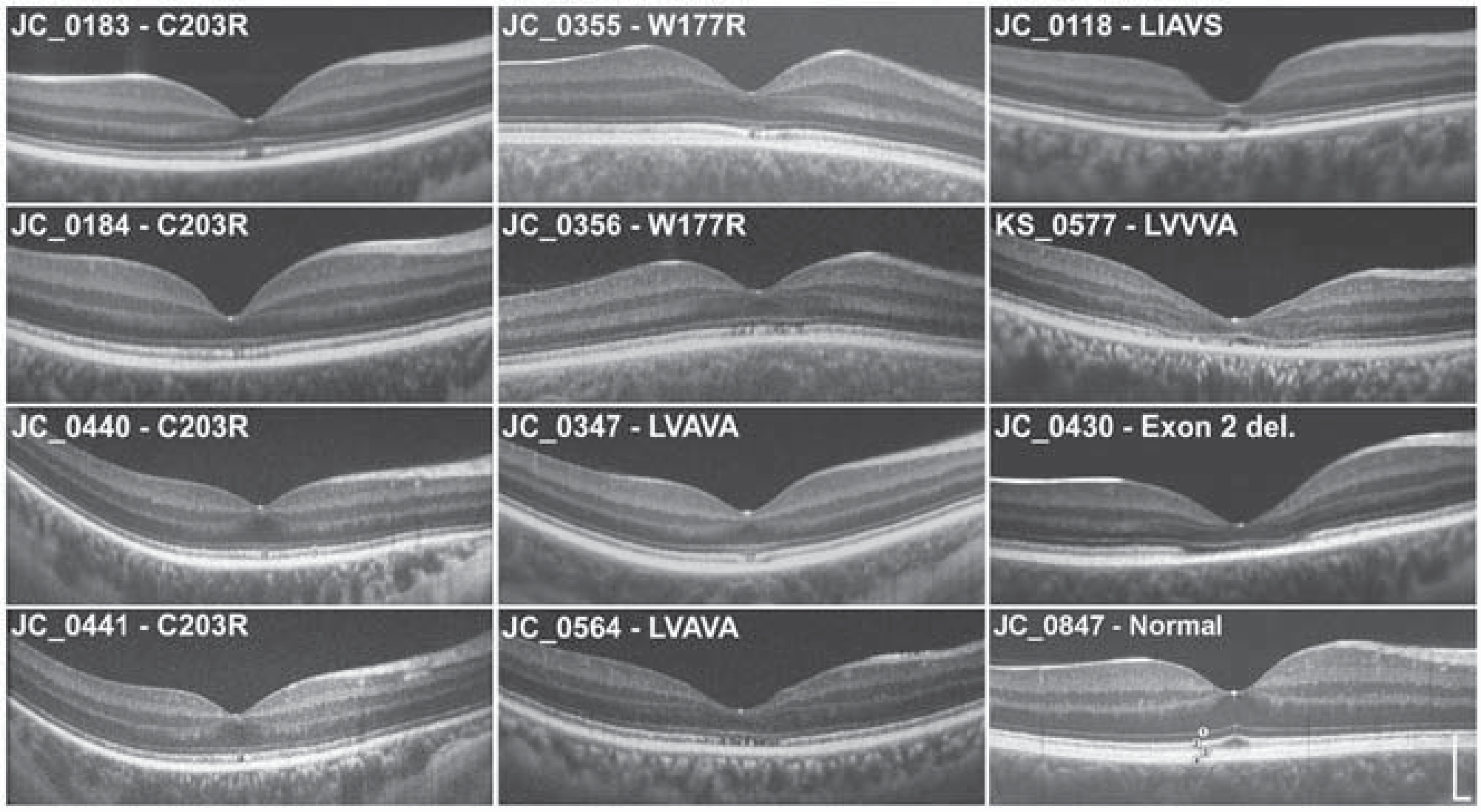
JC_0183 - C203R
JC_0355 - W177R
JC_0118 - LIAVS
JC_0184 - C203R
JC_0356 - W177R
KS_0577 - LVVVA
JC_0440 - C203R
JC_0347 - LVAVA
JC_0430 - Exon 2 del.
JC_0441 - C203R
JC_0564 - LVAVA
JC_0847 - Normal

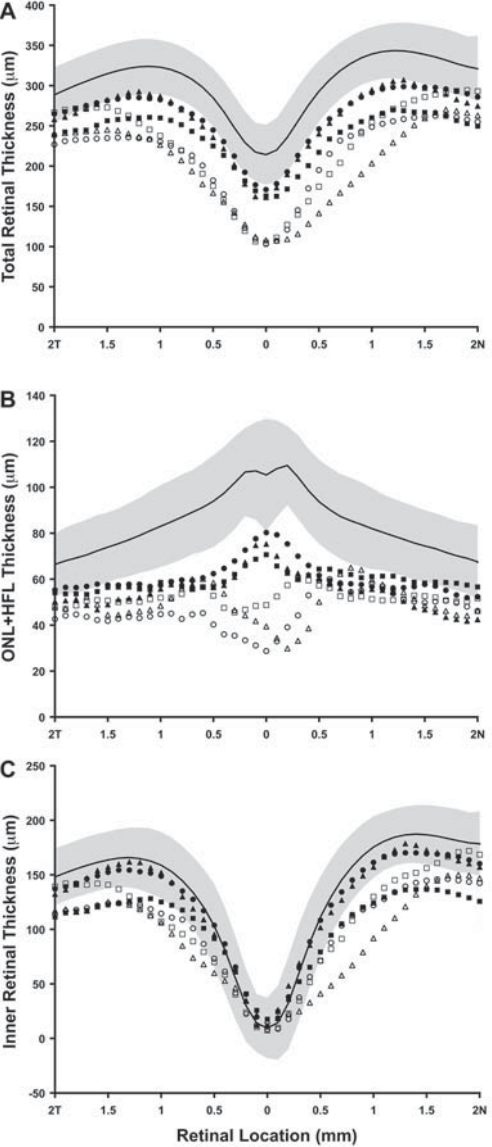
A
Total Retinal Thickness (μm)
400
350
300
250
200
150
100
50
0
2T
1.5
1
0.5
0
0.5
1
1.5
2N
B
ONL+HFL Thickness (μm)
140
120
100
80
60
40
20
0
2T
1.5
1
0.5
0
0.5
1
1.5
2N
C
Inner Retinal Thickness (μm)
250
200
150
100
50
0
-50
2T
1.5
1
0.5
0
0.5
1
1.5
2N
Retinal Location (mm)

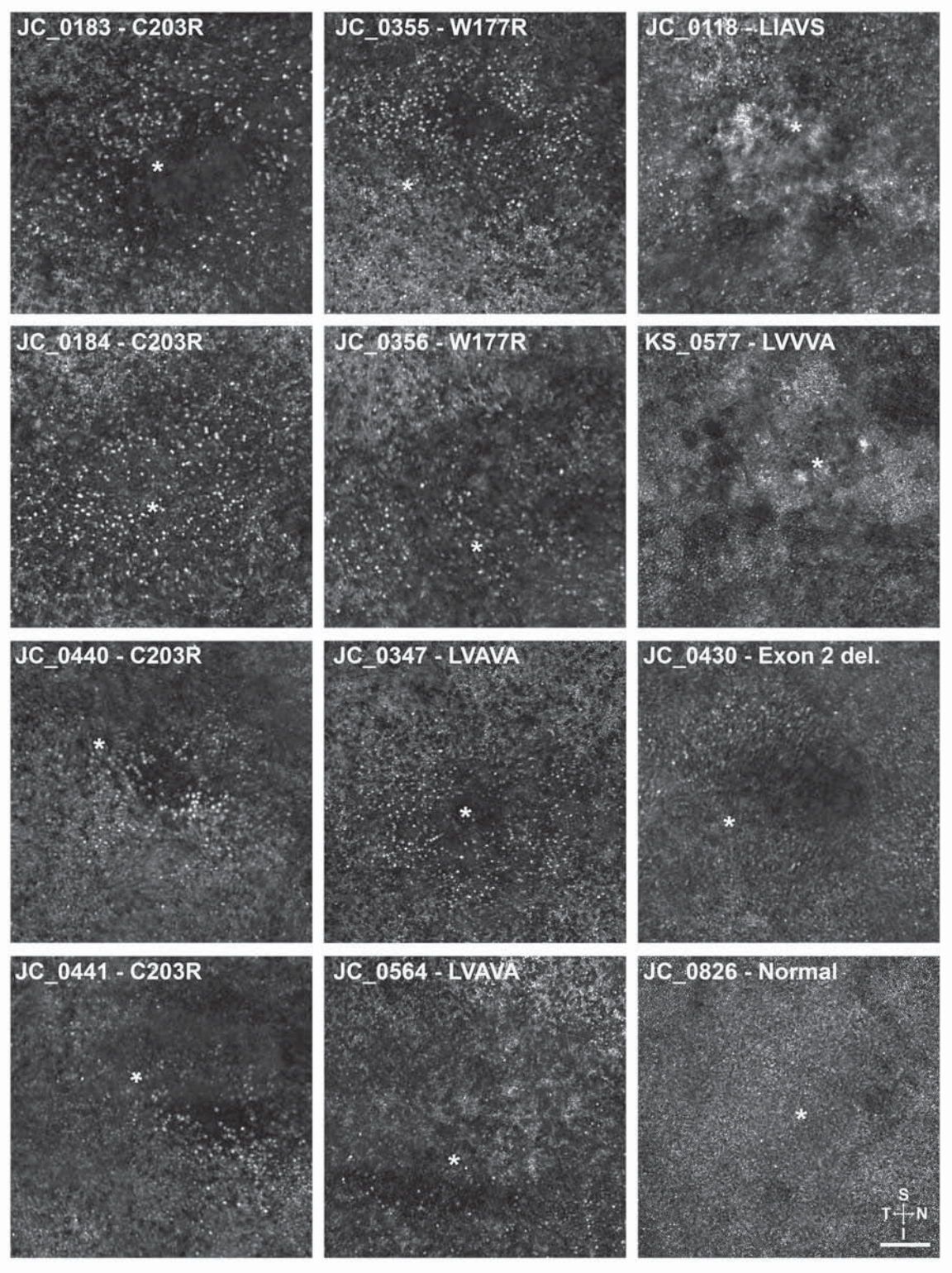
JC_0183 - C203R
JC_0355 - W177R
JC_0118 - LIAVS
JC_0184 - C203R
JC_0356 - W177R
KS_0577 - LVVVA
JC_0440 - C203R
JC_0347 - LVAVA
JC_0430 - Exon 2 del.
JC_0441 - C203R
JC_0564 - LVAVA
JC_0826 - Normal
S
T
N
I

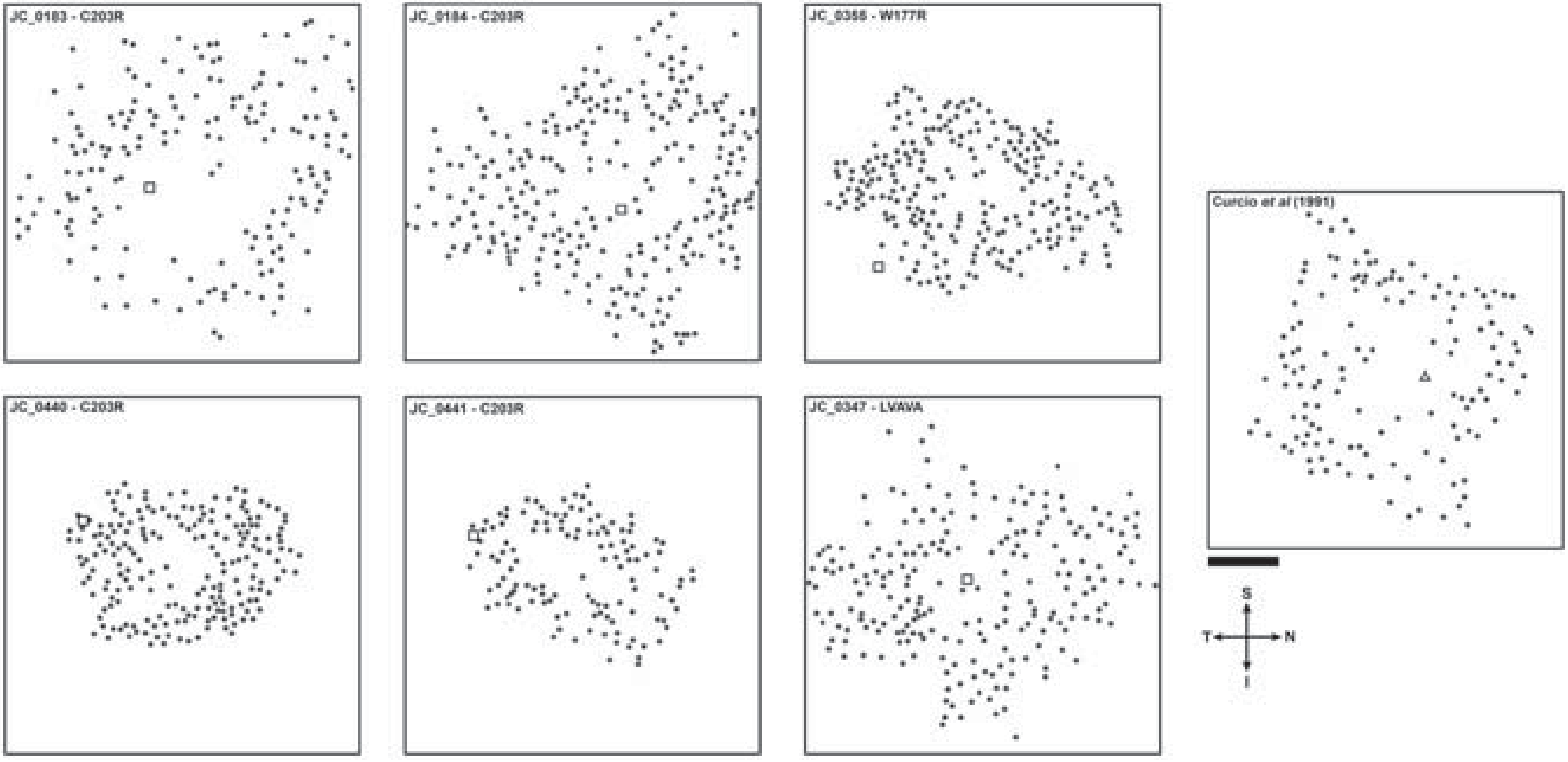
JC_0183 - C203R
JC_0184 - C203R
JC_0355 - W177R
Curcio et al (1991)
JC_0440 - C203R
JC_0441 - C203R
JC_0347 - LWWA
S
T
N
I

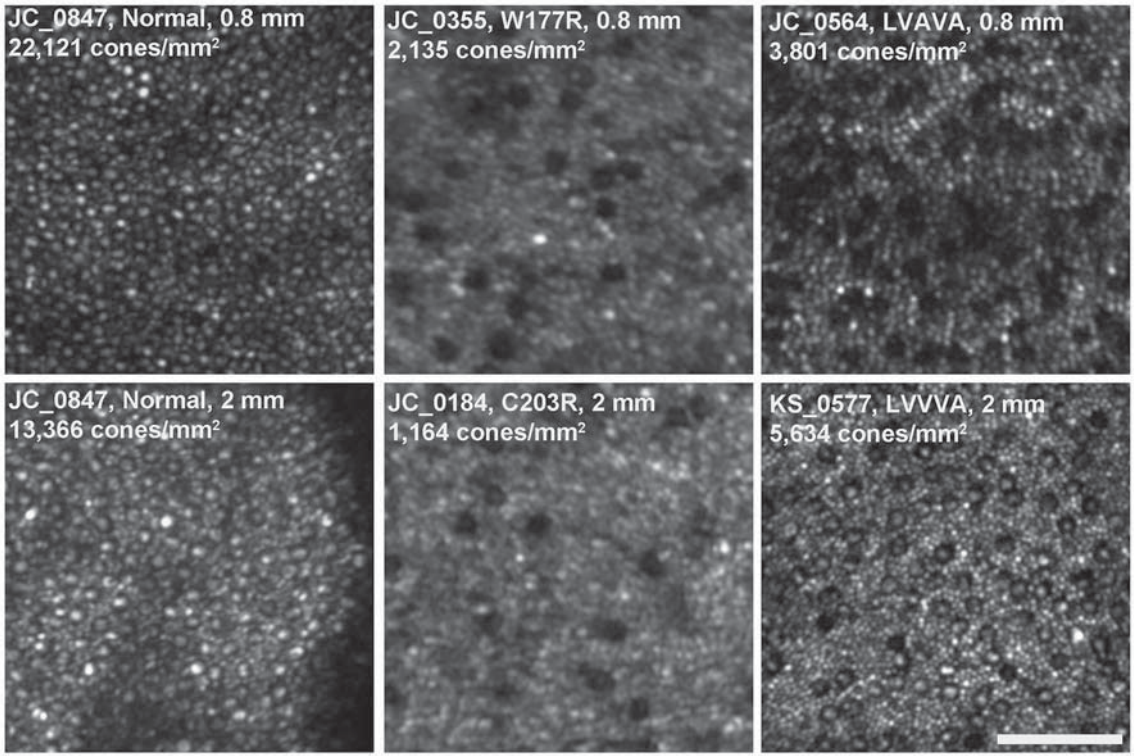
JC_0847, Normal, 0.8 mm
22,121 cones/mm²
JC_0355, W177R, 0.8 mm
2,135 cones/mm²
JC_0564, LVAVA, 0.8 mm
3,801 cones/mm²
JC_0847, Normal, 2 mm
13,366 cones/mm²
JC_0184, C203R, 2 mm
1,164 cones/mm²
KS_0577, LVVVA, 2 mm
5,634 cones/mm²

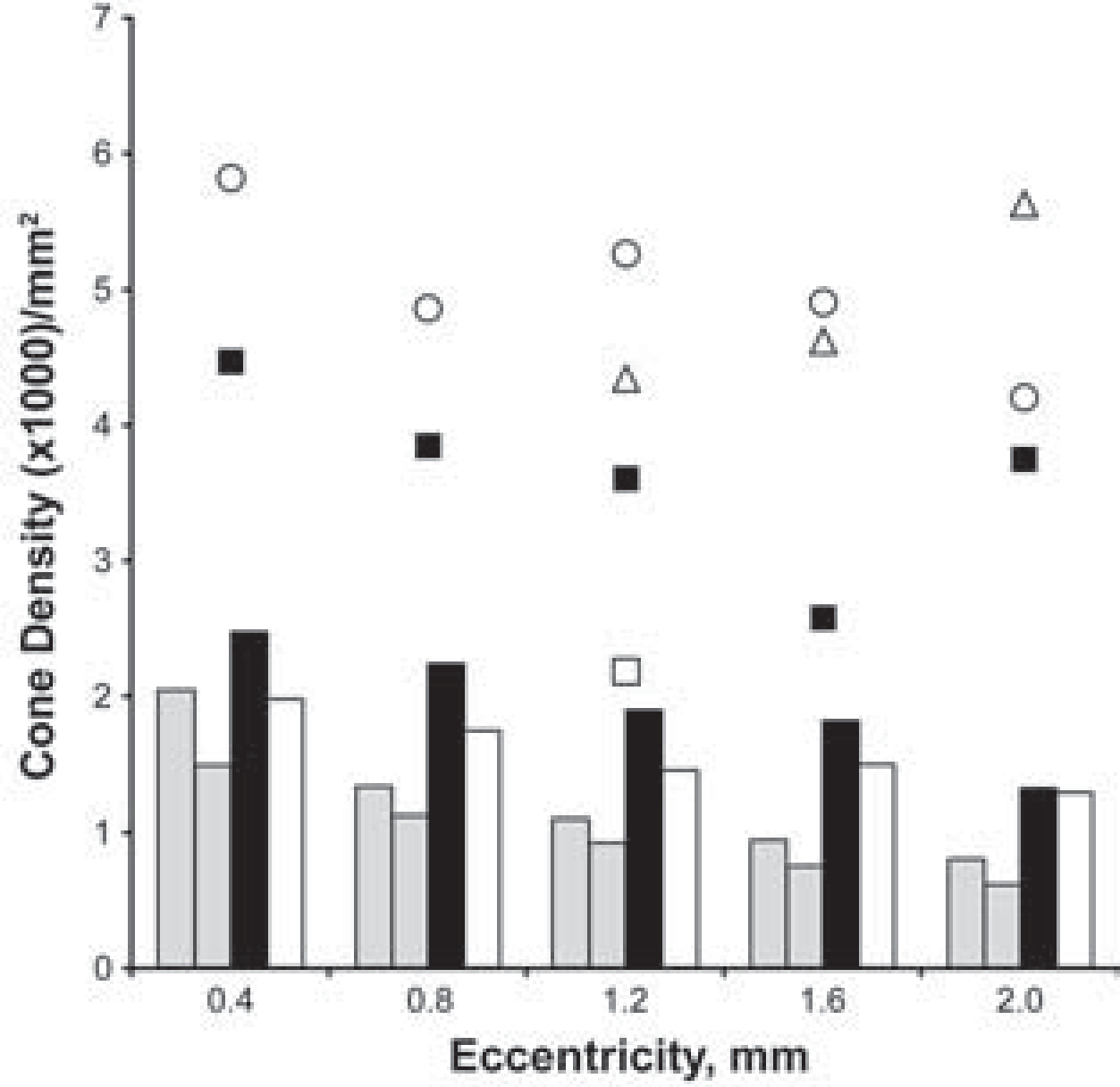
Cone Density (x1000)/mm²
7
6
5
4
3
2
1
0
0.4
0.8
1.2
1.6
2.0
Eccentricity, mm

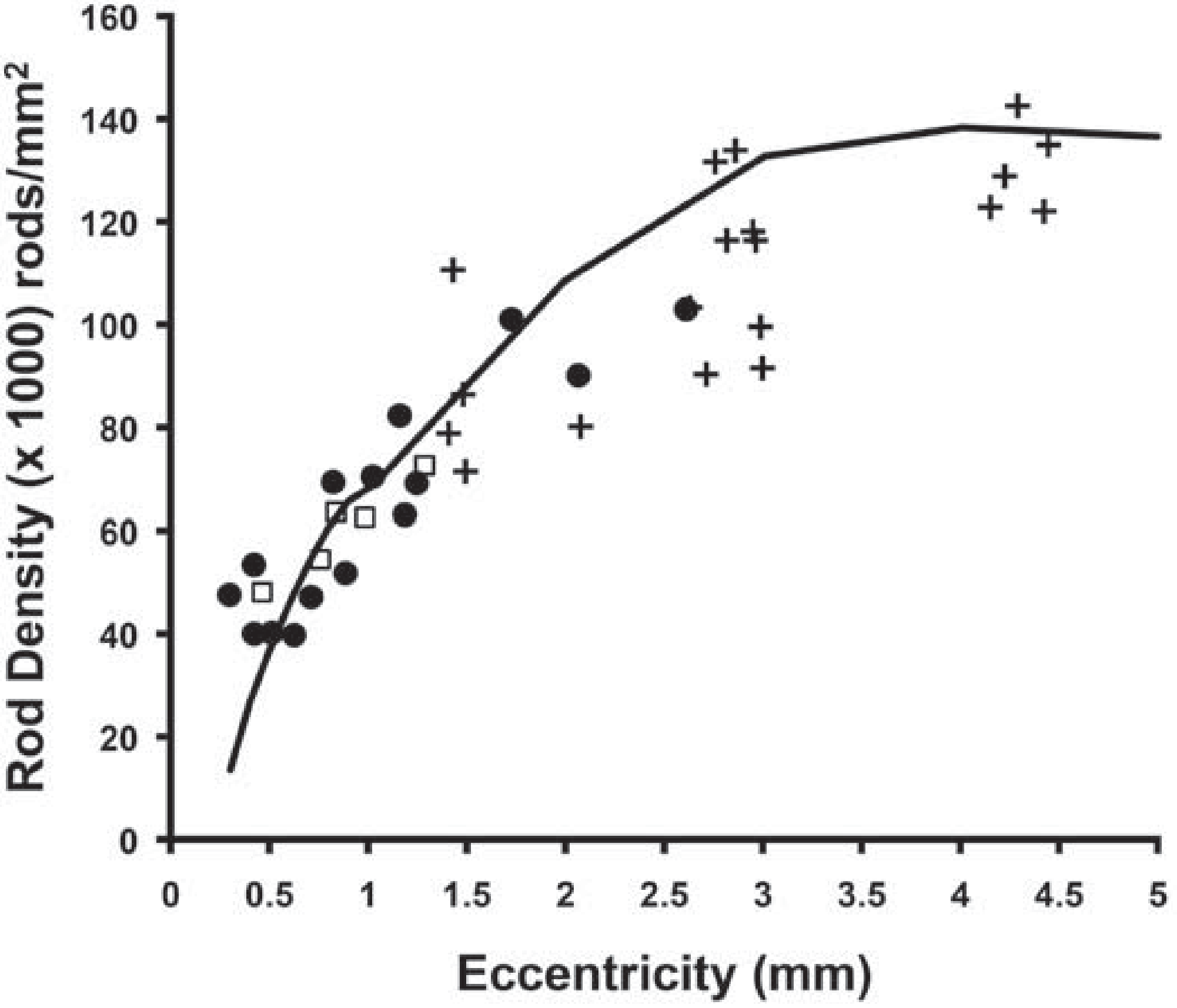
Rod Density (x 1000) rods/mm2
160
140
120
100
80
60
40
20
0
0
0.5
1
1.5
2
2.5
3
3.5
4
4.5
5
Eccentricity (mm)